# The Precipitation of the *Q* Phase in an AA6111 Alloy

G.C. WEATHERLY, A. PEROVIC, N.K. MUKHOPADHYAY, D.J. LLOYD, and D.D. PEROVIC

The precipitation behavior of the quaternary *Q* phase in an Al 6111 alloy has been studied by analytical electron microscopy. The transformation strain associated with the *Q* phase has been determined from high resolution electron microscopy and electron diffraction. The habit plane of the *Q* laths is shown to be fully coherent with the Al matrix. The transformation strain is used to explain the pattern of heterogeneous precipitation of the *Q* phase at dislocations and grain boundaries. The crystal structure and composition of the *Q* phase, whether it forms in the matrix or at grain boundaries, appears similar to that formed directly from the melt in a quaternary Al-Cu-Mg-Si alloy.

## I. INTRODUCTION

THE quaternary *Q* phase was first identified some 70 years ago[1] in Al-Mg-Si-Cu alloys from its etching response in optical metallography, at a time when the physical metallurgy community first became interested in precipitation strengthening. A spread of compositions ranging from $Al_4CuMg_5Si_4$ to $Al_4Cu_2Mg_8Si_7$ was suggested for the *Q* phase in subsequent studies,[2,3,4] but to this day, there is some uncertainty as to whether the *Q* phase has a unique composition in the quaternary Al-Cu-Mg Si system, or forms with a range of stoichiometries dependent on the alloy composition or heat treatment. The crystal structure of the *Q* phase was established by Arnberg and Aurivillius[5] using single crystals grown from a slowly cooled melt. The composition of the crystals was $Al_4Cu_2Mg_8Si_7$, with a hexagonal unit cell, $a = 1.03932$ nm, and $c = 0.40173$ nm. These same authors suggested that the diffraction data could be fitted to either the $P6_3/m$ or $P\bar{6}$ space group. These two possibilities can be distinguished by the presence or absence of $(0002n + 1)$ reflections, although X-ray structure factor calculations show that these reflections, if present, would be very weak. However, Arnberg and Auruvillius[5] chose the latter space group, as it led to a better overall fit with their diffraction data, despite the absence of (0001) reflections.

There has been a resurgence of interest in the *Q* phase over the past 10 years with the realization that it precipitates in many of the 6xxx series of age-hardened *A*l alloys being developed for automotive sheet applications.[6–10] The phase is reported to form with a unique orientation relationship with the matrix, *viz.*

$$[0001]_Q \,//\, [001]_{Al} \text{ and } [\bar{1}\bar{1}20]_Q \,//\, [510]_{Al}$$

giving 12 variants.[6,7] It grows as lath-shaped particles along $\langle 100 \rangle$ directions in the matrix. This observation has been rationalized by noting that the $\langle c \rangle$ lattice parameter of the *Q* phase, 0.402 nm, is nearly identical to the lattice parameter of Al, 0.405 nm. Indeed, the *Q* phase is often observed to be fully coherent with the matrix in these directions, leading to the designation of a *Q′* phase with $\langle c \rangle = 0.405$ nm.[7] However, the crystal structure of this phase is probably identical to the *Q* phase, and it is more correctly described as a coherent or semicoherent precipitate, constrained by its morphology and size to have an identical lattice parameter to Al along the growth direction. Another interesting feature of the precipitate morphology is the observation of {510} habit planes for the laths, consistent with the close matching in the repeat distances for the *Q* phase and Al in the habit plane.[7] While the crystal structure and morphology of the *Q* phase have been extensively explored, the factors controlling the nucleation of the phase remain obscure. In a recent study of a SiC-reinforced Al-Cu-Mg alloy, Cayron *et al.*[11] found two new phases, *QC* and *QP*, structurally similar to the *Q* phase, which they suggest could continuously transform from one phase to the other. In particular, the *QC* phase could be a precursor in the formation of the *Q* phase, although this hypothesis remains to be proven in Al-Cu-Mg-Si alloys.

The aim of the present study was to use high resolution transmission electron microscopy (HRTEM), coupled with a detailed composition analysis, to study the precipitation of the *Q* phase, to determine the interface structure, and to assess the stress-free transformation strain that describes the precipitation of this phase. The alloy used for the study was the Al-based alloy AA6111. A preliminary account of the precipitation behavior in this alloy, as well as in AA6016, identifying the roles played by the *Q* and $\beta''$ phases, has been presented elsewhere.[12] In that study, the emphasis was on the use of HRTEM studies to distinguish between the *Q* phase and the $\beta''$ phase. As the structure of the metastable $\beta''$ phase has been fully described by Anderson *et al.*[13] only the *Q* phase will be discussed in this article.

## II. EXPERIMENTAL PROCEDURE

The composition of the AA6111 alloy used to study the precipitation of the *Q* phase is listed in Table I. The alloy was first cast as a 600-mm-thick ingot, scalped to remove the shell zone, homogenized at 550 °C, hot rolled to about 2.5-mm-thick sheet, and finally cold rolled to 1-mm thickness. The cold-rolled sheets were then solution heat treated at 535 °C for 10 minutes, followed by either quenching or forced air-cooling to room temperature. A variety of heat treatments were employed in the study. The characterization of the interface structure of the *Q* phase was done using

G.C. WEATHERLY, Professor, is with the Department of Materials Science and Engineering, McMaster University, Hamilton, ON, Canada L8S 4M1. A. PEROVIC, Research Associate, and D.D. PEROVIC, Professor, are with the Department of Metallurgy and Materials Science, University of Toronto, Toronto, ON, Canada M5S 1A4. N.K. MUKHOPADHYAY, Reader, is with the Department of Metallurgical Engineering, Banaras Hindu University, Varanasi 221005, India. D.J. LLOYD, Senior Scientist, is with the Kingston Research and Development Center, Alcan International Ltd., Kingston, ON, Canada K7L 5L9.

Manuscript submitted July 5, 2000.

**Table I. Chemical Compositions of AA6111 (Weight Percent)**

| Mg | Si | Cu | Fe | Mn | Cr | Ti | Al |
|---|---|---|---|---|---|---|---|
| 0.75 | 0.63 | 0.75 | 0.05 | 0.05 | 0.06 | 0.06 | balance |

overaged samples that had been heat treated at 315 °C for times that ranged from 15 minutes to 24 hours. Grain boundary precipitation was detected in all the solution-treated samples, but the results presented in Section III come from samples that had been cooled by forced air, without further heat treatment. The first evidence of (heterogenous) matrix precipitation of the *Q* phase was found in samples that had been aged for 0.5 hours at 180 °C. A more complete discussion of the sequence of precipitation in this alloy is given in References 10 and 12.

In addition to studying *Q* phase precipitates, a quaternary alloy, identical in composition to that used by Arnberg and Aurivillius,[5] was prepared by induction melting and casting the alloy in a protective atmosphere. We were unable to isolate large *Q* phase crystals from this cast alloy, as it was a fine-grained mixture of $Mg_2Si$, $CuAl_2$, Si, and the *Q* phase. Samples were prepared for electron microscopy by grinding and collecting the resultant powder on holey C films. Grains of the *Q* phase were identified by energy dispersive X-ray analysis (EDX). These grains were then used for convergent beam electron diffraction (CBED) and HRTEM studies. This procedure allowed a comparison of the *Q* phase as formed by precipitation in the alloy and directly from the melt. More importantly, the CBED and HRTEM studies of the powder sample could be done on single grains of the *Q* phase without interference from the surrounding Al matrix. In the alloy, the latter effect can lead to ambiguities in interpretation of the HRTEM images.

Both the powder samples and the heat-treated alloy samples were analyzed using a conventional PHILIPS CM-12 electron microscope operating at 120 kV and a high resolution FEG JEOL*-2010 electron microscope, equipped with an EDX Link system, operating at 200 kV.

*JEOL is a trademark of Japan Electron Optics Ltd., Tokyo.

## III. RESULTS

### A. *Q Phase Powder Samples*

The composition of the *Q* phase, as determined (in weight percent) by the thin film approximation,[14] was 14.7 ± 1.2 pct Al, 21 ± 3.4 pct Cu, 32.5 ± 2.3 pct Mg, and 31.8 ± 1.7 pct Si, close to the calculated values of 17.2 pct Al, 20.3 pct Cu, 31.1 pct Mg, and 31.4 pct Si, quoted by Arnberg and Aurivillius[5] from their single-crystal studies. When the scatter in the EDX measurements, based on 33 individual readings, is accounted for, the compositions of the *Q* phase in the two studies are essentially identical. This result suggests that the *Q* phase in the quaternary system is a point compound. However, other studies[6,12] have found that a phase that appears crystallographically identical to the *Q* phase forms in Cu-free 6xxx alloys, so we cannot yet rule out the possibility that the *Q* phase spans a wide composition range. The CBED and selected area diffraction (SAD) diffraction patterns were recorded from a large number of crystal zone axes belonging to the [*hki*0] family, each of which contains the systematic (000$\ell$) row of reflections. Evidence was found for (0001) reflections at zone axes where there is no possibility of double diffraction giving rise to the (0001) reflection (refer to Figure 1 for an example of this). The electron diffraction evidence supports the conclusion reached by X-ray diffraction[5] that the space group of the *Q* phase is $P\bar{6}$.

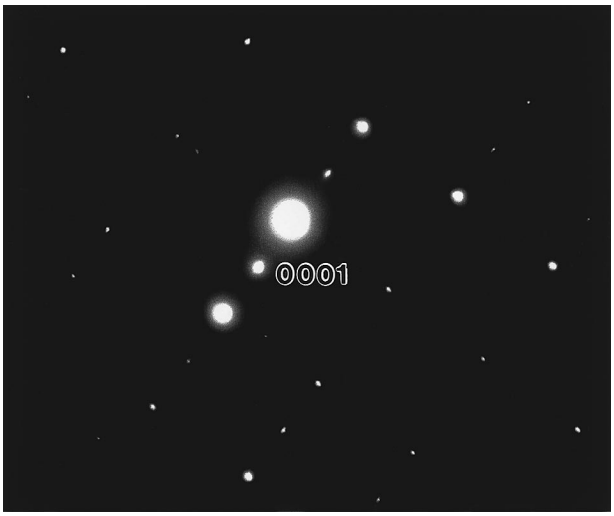


Fig. 1—Selected area diffraction pattern from [14$\bar{5}$0] zone axis of *Q* phase grain, showing the presence of (0001) reflections.

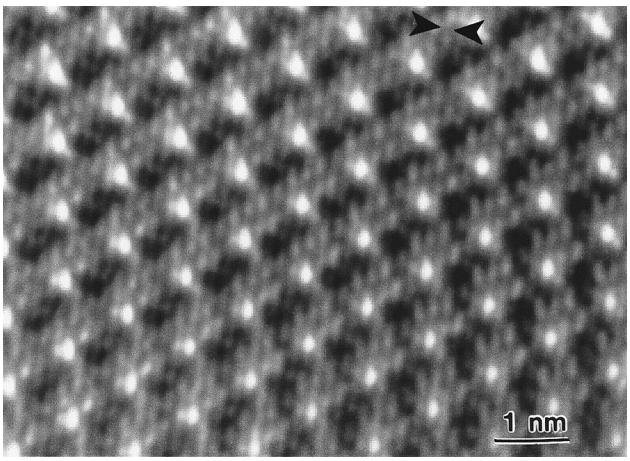


Fig. 2—HRTEM image from a [0001] oriented grain of the *Q* phase. A set of ($\bar{5}$140) planes is marked by arrows.

A number of HRTEM images were recorded from different zone axes. Figure 2 shows a typical example. All of the images could be explained by the known crystal structure of the *Q* phase,[5] when the crystal thickness and defocus values of each image were correctly accounted for. No evidence was found for any defect or faulted structures in the phase.

### B. *Overaged Structures*

The *Q* phase forms as laths lying along ⟨100⟩. In cross section, the laths show a prominent (flat) habit plane, {510},

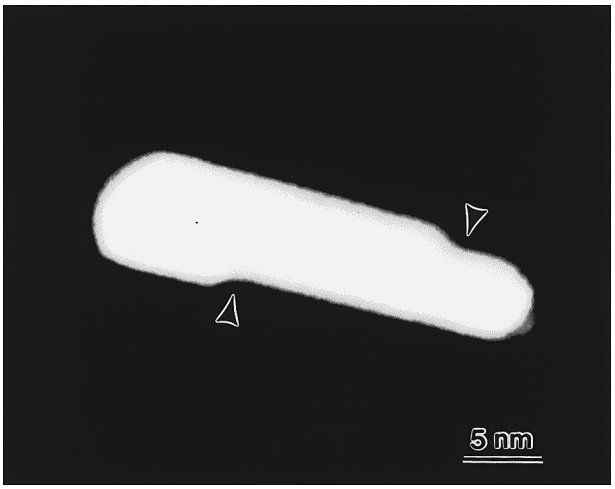


Fig. 3—Dark-field image showing the cross section of *Q* lath, with prominent $(510)_{Al}$ habit planes and ~1 nm high steps marked by arrows.

and irregular side facets (Figures 3 and 5). If the TEM thin foil sample is oriented along a $\langle 100 \rangle$ zone axis, the precipitates lie along one of the [0001], $[\bar{5}140]$, or $[1\bar{3}20]$ zone axes in the *Q* phase. Figures 4(a) and (b) show HRTEM images recorded from the *Q*-phase particles at the first two of these zone axes, taken under conditions where the particles extend through the thickness of the foil so that there is no interference from the Al matrix. (The HRTEM images shown throughout the article were first recorded on film as photographic images and then filtered using the inverse fast Fourier transform technique, allowing information out to $\mathbf{g}_{220}$ for Al in forming the final image.) Figure 4(c) shows for comparison a HRTEM image along the $[\bar{5}140]$ zone axis, taken under conditions where both the *Q* phase and Al lattices are contributing to the final image. At first sight, the image might be interpreted as coming from a regularly faulted structure, with the faults being spaced approximately 1 nm apart. However, standard (bright- or dark-field) images also show 1 nm spaced fringes under multiple $\langle 001 \rangle$ zone axis imaging conditions. The simplest interpretation is that these are moiŕe fringes, formed from the overlapping of the nearly parallel $(2\bar{6}40)$ and (200) reflections from the Q and Al phases. These planes have spacings of 0.1689 and 0.2025 nm, respectively, giving a moiré spacing of 1.02 nm.

The interface between the *Q* laths and the Al matrix is best studied in cross section, with the long axis of the precipitate, the $\langle c\text{-axis} \rangle$, parallel to the electron beam. Figure 5 shows two different examples of HRTEM images taken at this orientation. The orientation relationship between the two phases is identical to that given by Sagalowicz *et al.*[6] and Chakrabarti *et al.*[7] In Figure 5(a), a flat habit plane interface lying parallel to the $(510)_{Al}$ and $(1\bar{1}00)_Q$ planes in the two crystals is seen. The interface is defect free and there is perfect plane matching from correlated sets of planes across the interface.[15] The plane matching of the $(200)_{Al}$ and $(4\bar{5}10)_Q$ sets of planes, inclined at about 11 deg to the habit plane, has been marked on the figure to illustrate this point. The image of a stepped interface is shown in Figure 5(b). In this figure, the terraces correspond to the $(510)_{Al}$ habit plane, while the steps are about 0.9 nm in height, consistent with the spacing of the $(1\bar{1}00)$ planes in the *Q* structure. There has to be a misfit associated with each step

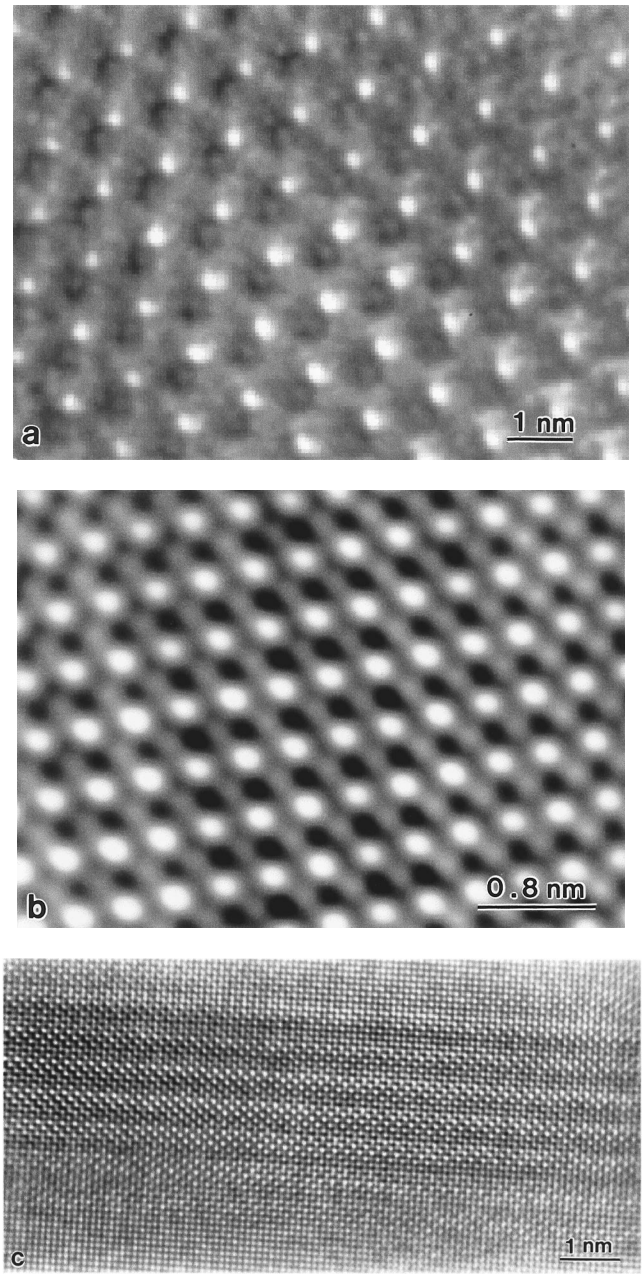


Fig. 4—HRTEM images from *Q* phase (*a*) [0001] zone axis, (*b*) $[\bar{5}140]$ zone axis, and (*c*) $[\bar{5}140]$ zone axis, where overlap of the *Q* phase and Al matrix has led to the formation of moiré fringes superimposed on the HRTEM image.

(required to bring the $(510)_{Al}$ and $(1\bar{1}00)_Q$ planes into perfect registry on each terrace); unfortunately, the quality of the HRTEM images at the step edges was not high and we could not distinguish between an elastic accommodation process of this misfit or accommodation by the introduction of misfit dislocations.

### C. *Grain Boundary Precipitation*

All the grain boundary precipitates found in this study (irrespective of the heat treatment) were *Q* phase, having the same orientation with one of the bounding grains as the matrix precipitates. Figure 6(a) shows a typical example

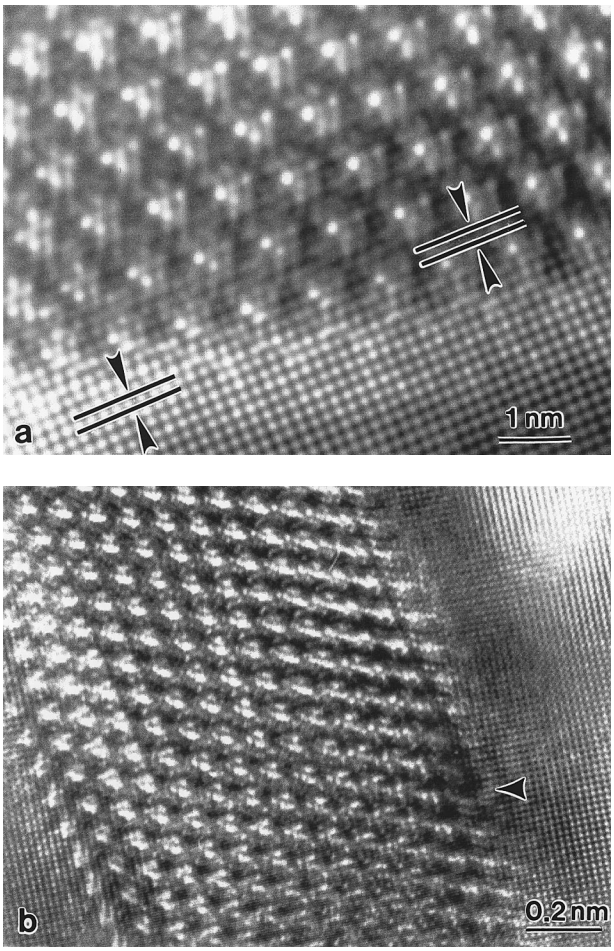


Fig. 5—HRTEM image from end-on *Q* phase, showing the structure of the $(510)_{Al}$ habit plane. (*a*) Flat habit plane, showing matching of the $(200)_{Al}$ and $(4\bar{5}10)_Q$ planes at the interface; and (*b*) habit plane with a 0.9-nm-high step (marked by arrow) connecting $(510)_{Al}$ terraces.

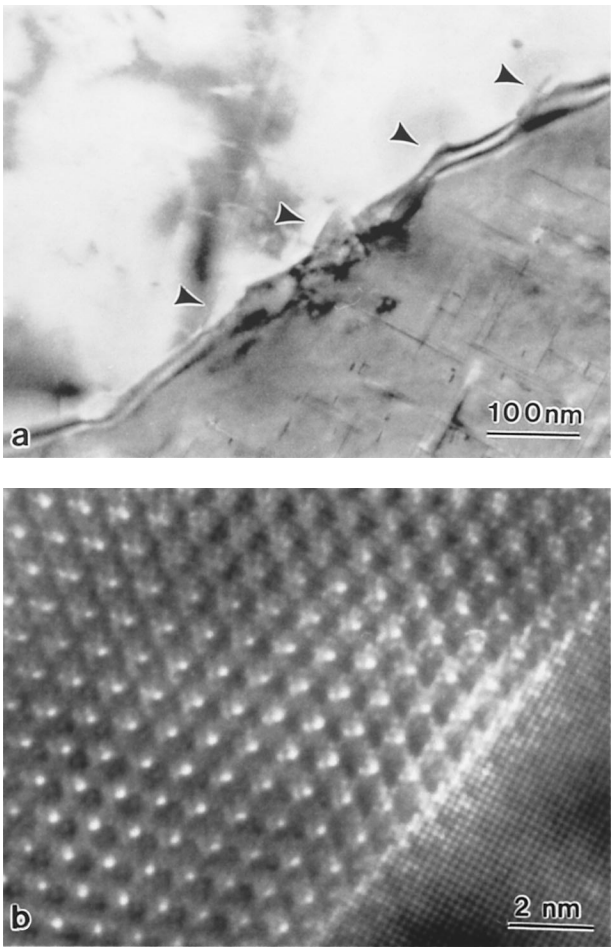


Fig. 6—(*a*) Bright-field image of *Q* phase precipitates at grain boundary in force air-cooled sample. (*b*) HRTEM image of $(510)_{Al}$ interface from a single grain boundary nucleated particle seen in (a).

from the sample that was force air-cooled. The precipitation has caused the grain boundary plane to "pucker" and the precipitate itself has grown into the grain with which it has the preferred orientation relationship. The major facet plane displayed by the particle corresponds to the $(510)_{Al}$ habit plane found with the matrix precipitates, as seen in the HRTEM micrograph of Figure 6(b).

Further proof of the similarities between the matrix and grain boundary *Q* phase is presented in Figure 7. Here, the EDX data from the grain boundary particles in peak-aged alloys and matrix particles in an overaged alloy (15 minutes or 24 hours at 315 °C) have been plotted according to the procedure proposed by Lorimer *et al.*[16] This method allows one to account for the effects of the Al matrix when there are overlap problems in the analysis, and, by extrapolation, to obtain the composition of the embedded phase. The two sets of data shown in Figure 7 yield identical values for the composition of the *Q* phase for both the matrix and grain boundary precipitates, *viz.* 33 pct Mg, 27 pct Si, 21 pct Cu, and 19 pct Al.

### D. *Precipitation on Dislocations*

The first precipitation of the *Q* phase in the matrix occurs heterogeneously on dislocations. The example shown in Figure 8 illustrates precipitation at a screw dislocation, $b = a/2[110]$. At low magnification (Figure 8(a)), the dislocation has a characteristic "wavy" contrast. At high magnification (Figure 8(b)), two variants of the *Q* phase, lying along [100] and [010], have nucleated at segments of the dislocation where locally the dislocation line is parallel to the long axis of the laths. The composition of the dislocation-nucleated particles, as measured by EDX, always contained Cu (Figure 8(c)), consistent with their designation as the *Q* phase. As there are six $a/2\langle 110\rangle$ dislocations and 12 variants of the *Q* phase, one expects from crystallographic considerations alone that at least two variants of the *Q* phase would nucleate at each dislocation, as observed. The details of the crystallography associated with this behavior are considered in the discussion.

## IV. DISCUSSION

### A. *The Transformation Strain Associated with Precipitation*

One of the key factors that determines many of the properties associated with a precipitate, *e.g.*, its nucleation behavior, interface structure, and strengthening characteristics, is the nature of the transformation strain describing how the crystal structures of the two phases (the *Q* phase and Al in this study) are linked. When the precipitate has a simple-crystal structure,

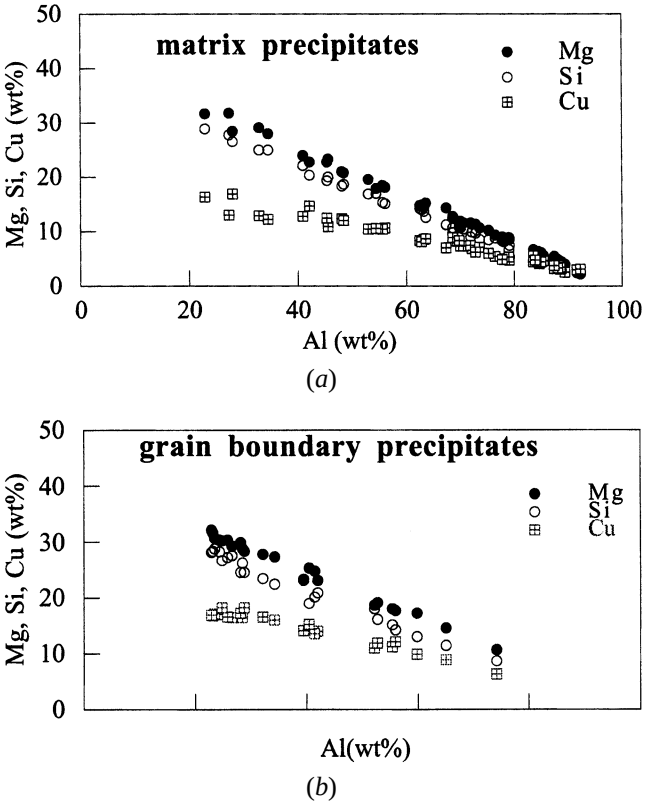


Fig. 7—Composition of the *Q* phase particles, as determined by EDX data, for matrix and grain boundary precipitates, and plotted according to the method suggested by Lorimer *et al.*[16]

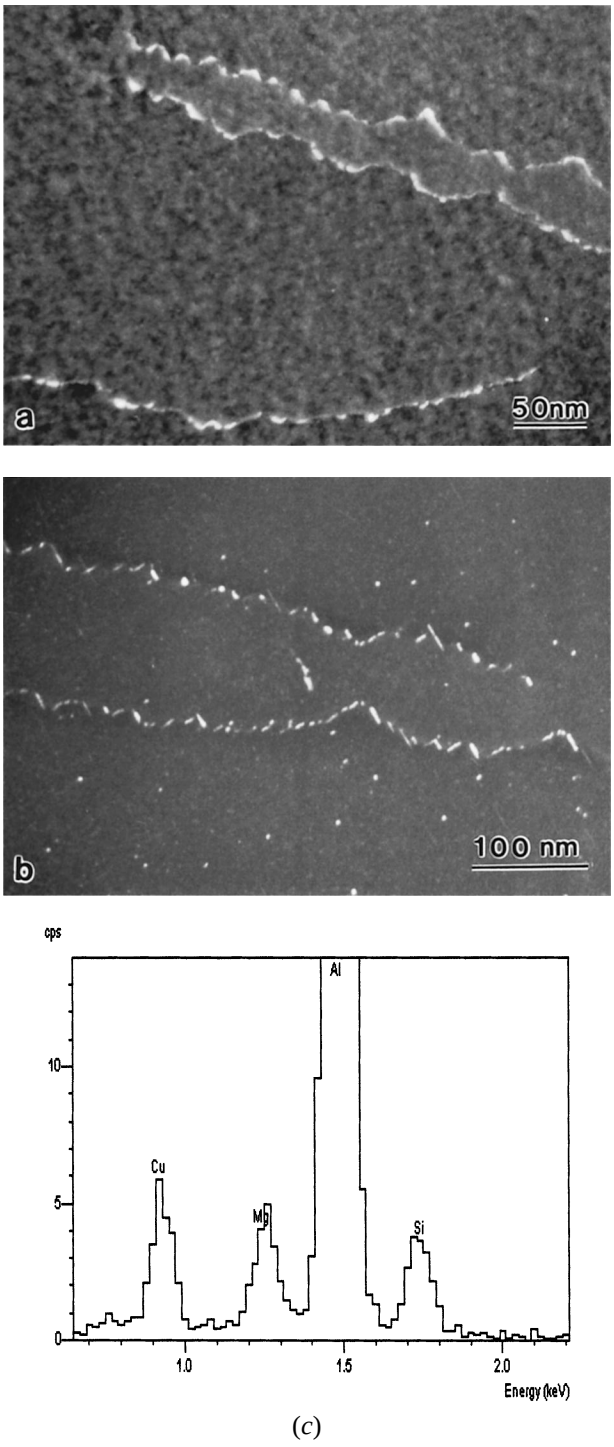


Fig. 8—Precipitation of the *Q* phase at dislocations in an alloy aged for 0.5 h at 180 °C. (*a*) dark-field image from matrix showing dislocation contrast; (*b*) dark-field image showing two variants of precipitates nucleated at the dislocations; and (*c*) EDX spectra from precipitates showing Cu, Mg, and Si peaks.

the transformation strain can be quickly determined from an inspection of the two lattices, but when the precipitate has a complex structure (as in the present case—the unit cell of the *Q* phase containing 21 atoms), the correspondence between the two lattices is not immediately transparent. In this section, we consider two approaches to this problem. Although the approaches attack the problem from different perspectives, they lead to the same conclusions.

The first method is based on the O-lattice or CSL, first introduced by Bollman,[17] and further developed in a series of articles by Zhang and co-workers.[18–21] These articles discuss the advantages of the information contained in electron diffraction patterns to determine whether a preferred low energy habit plane can be rationalized in terms of either the O-lattice or CSL approach. The method proposed by Zhang and co-workers[18–21] depends on finding one or more sets of $\Delta\mathbf{g}$ vectors that lie normal to a facet plane, where $\Delta\mathbf{g}$ is defined as the difference vector between two reflections, $\mathbf{g}_\alpha$ and $\mathbf{g}_\beta$, in the two lattices ($\alpha$ and $\beta$) bounding the interface. Thus, $\mathbf{g}_\alpha$ and $\mathbf{g}_\beta$ are said to be correlated if they are related by the transformation strain linking the two lattices. If $\mathbf{g}_\alpha$ and (or) $\mathbf{g}_\beta$ are low index, *e.g.*, (111) or (200) in the fcc lattice, the preferred habit plane corresponds to the condition where $|\Delta\mathbf{g}|$ is a maximum, as this leads to the lowest dislocation content (and energy) of the interface. As noted earlier, a preferred low energy habit plane will also lie normal to the $\Delta\mathbf{g}$ vectors. The correlated planes in this case correspond to $(\mathbf{g}_{200})_{\mathrm{Al}}$ and $(\mathbf{g}_{4\bar{5}10})_Q$, and $(\mathbf{g}_{020})_{\mathrm{Al}}$ and $(\mathbf{g}_{\bar{4}1\bar{5}0})_Q$. The $\Delta\mathbf{g}$'s lie normal to the $(510)_{\mathrm{Al}}$ habit plane provided the following geometric conditions are met: the angle between $\mathbf{g}_{200}$ and $\mathbf{g}_{4\bar{5}10}$ is 0.4 deg and the lattice parameter ratio $a_Q/a_{\mathrm{Al}}$ equals $(6.5)^{0.5}$. (There are other pairs of correlated $\mathbf{g}$'s that also can be used to define the habit plane following the same approach, *e.g.*, $\mathbf{g}_{060}$ and $\mathbf{g}_{105\bar{1}\bar{5}0}$. The latter plane lies perpendicular to $\mathbf{g}_{4\bar{5}10}$ and provides a link between a strain representation of the transformation, discussed subsequently, and the $\Delta\mathbf{g}$ approach). These predictions fit well to the experimental results. The deviation of 0.4 deg between the $(200)_{\mathrm{Al}}$ and

$(4\bar{5}10)_Q$ planes can be detected in the lattice image of Figure 5(a). The *a*-lattice parameter of the *Q* phase is predicted to be 1.033 nm, the value found by electron diffraction. The (510) habit plane contains a line $[1\bar{5}0]_{Al}$, parallel to $[11\bar{2}0]_Q$, across which there is perfect plane matching, as seen in the HRTEM image of Figure 5(a). Furthermore, as noted earlier, $[001]_{Al}$, parallel to $[0001]_Q$, is an effective invariant line, as the lattice parameter of the *Q* phase is elastically constrained to fit with the Al lattice in this direction.[7] The $(510)_{Al}$ interface is an invariant (fully coherent) plane, for the size range of *Q* particles we have examined in this study.

The more common method used in the literature to define an undistorted plane, in what is essentially a two-dimensional problem, is the strain ellipse approach,[22,23] where the parent phase (Al) is represented by a unit circle ($x^2 + y^2 = 1$) and the product phase (*Q*) by an ellipse ($x^2/a^2 + y^2/b^2 = 1$). The parameters *a* and *b* are related to the principal strains along the *x* [100] and *y* [010] axes needed to transform one lattice into the other. In the present case, if *a* and *b* are given by the ratios of the plane spacings ($d_{4\bar{5}10}/d_{200}$) and ($d_{105\bar{1}\bar{5}0}/d_{060}$), respectively, *i.e.*, $a = 0.9636$ and $b = 1.0014$, the $(510)_{Al}$ habit plane and deg rotation between these sets of planes can both be predicted from the analyses described in References 22 and 23, in full agreement with the $\Delta\mathbf{g}$ approach. The transformation from the Al to *Q* lattices is a plane strain deformation. For the variant with a $(510)_{Al}$ habit plane, the transformation can be formally described as a shear along $[1\bar{5}0]_{Al}$ with a dilatation of $(ab - 1)$ along $[510]_{Al}$.

### B. *Heterogeneous Nucleation*

The principles that govern the heterogeneous nucleation behavior of the *Q* phase follow those elucidated in a number of previous studies of Al alloys. For example, the most favorable condition for nucleation on dislocations corresponds to the situation where the maximum misfit vector of the precipitate is parallel or nearly parallel to **b**, and the dislocation line direction lies in the habit plane of the precipitate.[24,25] The behavior observed at the screw dislocation (Figure (8)) provides a clear illustration of these two rules. Segments of the original screw dislocation have moved by climb (and slip) so that they lie along $[100]_{Al}$ and $[010]_{Al}$ directions. These segments act as sites for heterogeneous nucleation of two variants of the *Q* phase, with the lath axis lying along $[100]_{Al}$ or $[010]_{Al}$, parallel in each case to the dislocation line. Since the maximum misfit vector of the *Q* phase is normal to the $\{510\}_{Al}$ habit plane of the lath (refer to earlier discussion), the two favored variants for the particular dislocation seen in Figure 8, $b = a/2[110]$, would be those having an $(051)_{Al}$ habit plane for [100] oriented laths and a $(501)_{Al}$ habit plane for [010] oriented laths.

Precipitation at grain boundaries always occurred with a preferred orientation relationship, identical to the relationship of the matrix *Q* phase, with one of the two bounding grains. If the grain boundary plane contained a ⟨100⟩ direction, the precipitate grew with a faceted morphology along that direction and maintained a $\{510\}_{Al}$ facet plane (Figure 6). If the grain boundary did not contain a ⟨100⟩ direction, the morphology of the *Q* phase was more equiaxed, but it still maintained the preferred orientation relationship with one of the two grains. These results are all explained by the theory of heterogeneous nucleation at grain boundaries,[26] which predicts that the most favored crystallographic variant(s) will be those that maximize the area of the low energy habit plane with one of the two grains.

## V. SUMMARY

The precipitation and morphology of the quaternary *Q* phase in an Al6111 alloy are controlled by the development of a fully coherent $(510)_{Al}$ habit plane, leading to lath-shaped particles lying along $\langle 100\rangle_{Al}$. The transformation strain associated with the precipitation of the *Q* phase is determined by three sets of correlated planes: $(200)_{Al}$ and $(4\bar{5}10)_Q$, $(020)_{Al}$ and $(\bar{4}\bar{1}50)_Q$, and $(002)_{Al}$ and $(0002)_Q$. The composition of the *Q* phase formed directly from a quaternary melt is similar to that formed by precipitation from a supersaturated solid solution.

## ACKNOWLEDGMENTS

The authors are grateful to Materials and Manufacturing Ontario (MMO) and to Alcan for their support of this work.

## REFERENCES

1. E.H. Dix, G.F. Sager, and B.P. Sager: *Trans. AIME*, 1932, vol. 99, pp. 119-29.
2. L.F. Mondolfo: *Metallography of Aluminum*, John Wiley, New York, NY, 1943, p. 249.
3. D.A. Petrov: *Acta Physicochimica, URSS*, 1937, vol. 6 (4), p. 505.
4. G.J. Phragmen: *J. Inst. Met.*, 1950, vol. 77, pp. 489-552.
5. L. Arnberg and B. Aurivillius: *Acta Chem. Scand. A*, 1980, vol. 34, pp. 1-5.
6. L. Sagalowicz, G. Lapasset, and G. Hug: *Phil. Mag. Lett.*, 1996, vol. 74, pp. 57-66.
7. D.J. Chakrabarti, B. Cheong, and D.E. Laughlin: in *Automotive Alloys II*, S.K. Das, ed., TMS, Pittsburgh, PA, 1998, pp. 27-44.
8. G.A. Edwards, K. Stiller, G.L. Dunlop, and M.J. Couper: *Acta Mater.*, 1998, vol. 46, pp. 3893-3904.
9. K. Matsuda, Y. Uetani, H. Anada, S. Tada, and S. Ikeno: *Proc. 3rd Int. Conf. on Aluminum Alloys*, L. Armburg, O. Lohne, E. Nes, and N. Ryum, eds., Norwegian Institute of Technology, Trondheim, 1992, vol. 1, p. 272.
10. A.K. Gupta and D.J. Lloyd: *Proc. 3rd Int. Conf. on Aluminum Alloys*, L. Armburg, O. Cohne, E. Nes, and N. Ryum, eds., 1992, vol. 2, p. 21.
11. C. Cayron, L. Sagalowicz, O. Beffort, and P.A. Buffat: *Phil. Mag. A*, 1999, vol. 79, pp. 2833-51.
12. A. Perovic, D.D. Perovic, G.C. Weatherly, and D.J. Lloyd: *Scripta Mater.*, 1999, vol. 41, pp. 703-08.
13. S.J. Andersen, H.W. Zandbergen, J. Jansen, C. Traeholt, U. Tundal, and O. Reiso: *Acta Mater.*, 1998, vol. 46, pp. 3283-98.
14. G. Cliff and G.W. Lorimer: *J. Microsc.*, 1975, vol. 103, pp. 203-7.
15. W.-Z. Zhang: *Proc. Int. Conf. on Solid-Solid Phase Transformations '99 (JIMIC-3)*, M. Koiwa, K. Ostuka, and T. Miyazaki, eds., Japan Institute of Metals, Sendai, Japan, 1999, p. 581.
16. G.W. Lorimer, G. Cliff, P.E. Champness, C. Dickinson, F. Hansan, and P. Kenway: in *Analytical Electron Microscopy*, D.B. Williams and D.C. Joy, eds., San Francisco Press, San Francisco, CA, 1984, p. 153.
17. W. Bollmann: *Crystal Defects and Crystalline Interfaces*, Springer, Berlin, 1970.
18. W.-Z. Zhang and G.R. Purdy: *Phil. Mag.*, 1993, vol. 68A, pp. 279-90.
19. W.-Z. Zhang and G.R. Purdy: *Phil. Mag.*, 1993, vol. 68A, pp. 291-303.
20. D. Duly, W.-Z. Zhang, and M. Audier: *Phil. Mag.*, 1995, vol. 71A, pp. 187-204.
21. W.-Z. Zhang: *Phil. Mag.*, 1998, vol. 78A, pp. 913-33.
22. U. Dahmen: *Acta Metall.*, 1982, vol. 30, pp. 63-73.
23. V. Radmilovic, R. Kilaas, U. Dahmen, and G.J. Shiflet: *Acta Mater.*, 1999, vol. 47, pp. 3987-97.
24. A. Kelly and R.B. Nicholson: *Progr. Mater. Sci.*, 1963, vol. 10, pp. 149-391.
25. R.M. Allen and J.B. Van der Sande: *Acta Metall.*, 1980, vol. 28, pp. 1185-95.
26. J.K. Lee and H.I. Aaronson: *Acta Metall.*, 1975, vol. 23, pp. 799-808.